ACS MEASUREMENT SCIENCE Au
AN OPEN ACCESS JOURNAL OF THE AMERICAN CHEMICAL SOCIETY

pubs.acs.org/measureau
Article

In Situ Quantification of a Wetted Surface Area during Scanning Electrochemical Cell Microscopy Using Retraction Curves

Published as part of ACS Measurement Science Au special issue "2024 Rising Stars".

Nishtha Saxena, Emmanuel Mena-Morcillo, Mia Tripp, Peter George Keech, Mehran Behazin, and Samantha Michelle Gateman*

Cite This: ACS Meas. Sci. Au 2025, 5, 178–188
Read Online

ACCESS | Metrics & More | Article Recommendations | Supporting Information

ABSTRACT: This work presents a new methodology to estimate the surface area of the working electrode during scanning electrochemical cell microscopy (SECCM) *in situ* by utilizing retraction curves. In this approach, the current is measured as a function of pipet displacement in the *z*-direction. When the current drops to zero, it is indicative of droplet detachment from the surface, allowing for the estimation of the droplet contact diameter based on the pipet displacement. This enables real-time estimations of surface areas of the wetted electrode at each point of measurement, rather than performing time-consuming measurements using *ex situ* correlative image analysis or estimating an average working electrode size from the pipet aperture. Notably, during SECCM measurements on copper in nitric acid, the working electrode diameter estimated using retraction curves was significantly smaller than the droplet footprint diameter observed post experiment using *ex situ* correlative image analysis. This discrepancy is attributed to droplet spreading after pipet retraction, as confirmed by goniometer and silanized pipet measurements. Upon cleaning the surface, the true wetted surface areas during SECCM measurements were found to be in good agreement with values estimated using retraction curves yet were larger than the pipet aperture. Additionally, the effects of approach separation, retraction rates, and probe diameter on the droplet contact size were analyzed using retraction curves. These findings were compared to *ex situ* methods to assess the reliability of the retraction curves for determining the working electrode surface area. This study demonstrates the potential of retraction curves to provide a higher accuracy in the quantitative analysis of local current density values extracted using SECCM.

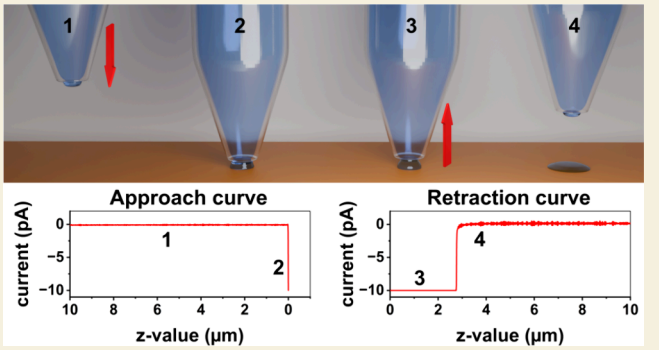

KEYWORDS: *scanning electrochemical cell microscopy, SECCM,, electrochemistry, copper, corrosion, retraction, surface area quantification, droplet measurements*

1. INTRODUCTION

Investigating corrosion phenomena that are related to specific microstructural features is challenging due to their localized nature in polycrystalline metals and coatings, such as surface grains[1] with varying crystallographic orientations,[2] grain boundaries,[3] and precipitates/inclusions.[4] Macroscopic electrochemical techniques measure surface-averaged responses of a material's corrosion behavior and do not provide quantitative localized information about corrosion mechanisms.[5−9] Therefore, electrochemical techniques that operate at the (sub)-microscale are needed to enable the precise correlation of electrochemical activity and surface structure and chemistry.

For decades, scanning electrochemical probe microscopy (SEPM) has been harnessed to elucidate local reactivity to the microstructure of corroding metals.[10] Scanning electrochemical microscopy (SECM) is the most popular technique for corrosion studies, where an ultramicroelectrode (UME) is rastered close to the corroding substrate while local electrochemical information is recorded.[11,12] Although a promising method, SECM does not directly measure the corrosion rate of the metal of interest and the method usually relies on a redox mediator in solution to probe local electrochemical reactivity.[13] In contrast, scanning electrochemical cell microscopy (SECCM) enables direct and local measurements of corrosion properties by enclosing the electrochemical cell within a small, freely hanging droplet formed at the tip of a micro- or nanopipet.[14,15] Although similar in principle to the electro-

Received: July 13, 2024
Revised: September 24, 2024
Accepted: September 26, 2024
Published: October 4, 2024

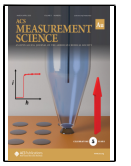

chemical droplet cell (EDC) developed by Suter and Böhni,[16,17] the SECCM setup offers several key advancements. While both techniques enable localized electrochemical analysis, the SECCM uses the advantage of a high-resolution positioning system coupled with a data acquisition system, allowing for direct and automated electrochemical imaging of corroding substrates at the micro- and nanoscale.[18−21] In contrast, the EDC method employed a larger microcell aperture, which used a silicone gasket to maintain droplet size and relied on manual positioning using an optical microscope. The SECCM's automation and probe flexibility provide significantly enhanced spatial resolution compared to the droplet cell.

Extracting the corrosion parameters at an individual microstructural feature is one of the benefits of SECCM, enabling the identification of the features that are most susceptible to corrosion.[22] To obtain quantitative corrosion rates, the current obtained during the polarization measurements must be normalized by the surface area of the working electrode. Unlike macroscale electrochemical and EDC measurements where the working electrode is isolated and its surface area is well-defined, the working electrode's surface area during SECCM measurements is determined by the size of the pipet aperture and the interaction between the wetted surface and the freely hanging droplet from the micro/nanopipet.

Due to differences in microstructure, morphology, and/or surface chemistry, the wettability of the surface may vary at each point of measurement and result in different surface areas isolated.[23] For instance, the change in the surface energy when the sample is electrochemically polarized can alter its wetting properties and result in different isolated surface areas at each point of measurement.[24] In addition, surface features such as polycrystalline grains, grain boundaries, and inclusions present in metals/alloys can possess different surface energies and result in heterogeneous wetting at each landing point.[25] Furthermore, different surface preparation procedures can result in different surface roughnesses, affecting the contact angles and modulating the droplet spread dynamics.[26] The exposure time of freshly polished metal to an atmosphere can also influence the surface's wetting properties, as atmospherically formed surface films (oxide films, adventitious carbon deposits) can greatly affect the surface energy.[27] Yet, most SECCM studies have estimated that the working electrode's surface area is equivalent to the pipet aperture.[28,29] Without considering wetting, this assumption may lead to an overestimation of the current density and, ultimately, corrosion rates.

Other studies have used *ex situ* techniques such as scanning electron microscopy (SEM)[2] or atomic force microscopy (AFM)[21] to measure the surface area of the droplet footprints (corroded area and/or electrolyte salt deposit) at each point of measurement. However, these methods become time-consuming when individually measuring the areas of hundreds to thousands of points. In addition, features of the surface may change during the drying and subsequent handling of the sample prior to its surface analysis, and it may be necessary to remove corrosion products of the electrochemical reaction to obtain accurate measurements of the surface area of the droplet. Hybrid SECCM-interference reflection microscopy (SECCM-IRM) is a promising technique for monitoring the droplet size during interfacial interrogation in real time.[30] However, it requires that the substrate be transparent, which metals and alloys are not. Therefore, there is a need for an alternative method that is both time-efficient and capable of precisely measuring the size of droplets during SECCM measurements.

This work outlines the development of a new methodology for monitoring the working electrode's surface area *in situ* during SECCM measurements by analyzing the retraction curves, the current measured as a function of pipet displacement from the substrates's surface. This quick method accurately estimates each droplet's contact diameter (the part of the substrate in contact with the droplet before retraction) *in situ* at each point of measurement. To demonstrate accuracy, the estimated droplet contact diameters from retraction curves were compared to the size of the pipet and the droplet footprint diameter (droplet traces on surface post SECCM measurements) *ex situ* using complementary microscopy methods. Various experimental parameters such as the effect of landing separation, retraction scan rates, and pipet aperture size were explored to validate the method.

The substrate selected for this study was wrought copper, as this work has particular relevance to the nuclear waste management community, which proposes to use copper as a coating material for used nuclear fuel containers.[31−33] Copper is also a very convenient model material owing to its overall stability as a quasi-noble metal and absence of truly passive oxide films within aqueous systems[34] and well-characterized electrochemical oxidation parameters.[35] The electrolyte chosen was nitric acid due to its formation under humid air radiolysis and anticipated presence upon the initial deposition of the used fuel containers underground.[36,37] To predict long-term corrosion phenomena of the copper coatings,[38] it is crucial to explore the relationship between the microstructure and corrosion behavior, in which SECCM will provide valuable future insights. Accurate estimation of droplet size in SECCM is important to determine the true surface area for reliable corrosion measurements, where this study on wrought copper lays the foundational work to ensure that reliable local electrochemical measurements are extracted using SECCM.

2. EXPERIMENTAL SECTION

2.1. Materials and Reagents

Wrought, phosphorus-doped, and oxygen-free Cu was supplied by Svensk Kärnbränslehantering (SKB). HNO_3 and HCl were purchased from Fisher Scientific (Ottawa, ON, Canada) and were used as an electrolyte and to remove corrosion products from the surface, respectively. All solutions were prepared using ultrapure water (18.2 MΩ-cm) from a Barnstead Nanopure Diamond Water Purification System (Dubuque, IA, USA). Ag wire of diameter 0.1 mm was purchased from Goodfellow (99.99% purity, Cambridge Limited, Huntingdon, England). Commercial bleach was purchased from Lavo Inc. (Montreal, Canada). Dichlorodimethylsilane (>99.5% purity) was purchased from Sigma-Aldrich.

2.2. Sample Preparation

Cu samples (dimensions: 2 × 2 × 1 cm) were polished using SiC abrasive papers with grits ranging from 400 to 4000, on a Metaserv 2000 Single Grinder Polisher from Buehler (Whitby, ON, Canada). The final polishing step was performed systematically using a 1 μm diamond polish solution to ensure consistency across the sample, resulting in a surface roughness parameter (Sa) of 0.018 μm. After being polished, the samples were thoroughly washed using ultrapure water followed by drying under argon. Conductive copper tape was used to make an electrical connection by fastening a wire to the sample.

https://doi.org/10.1021/acsmeasuresciau.4c00042
ACS Meas. Sci. Au 2025, 5, 178−188

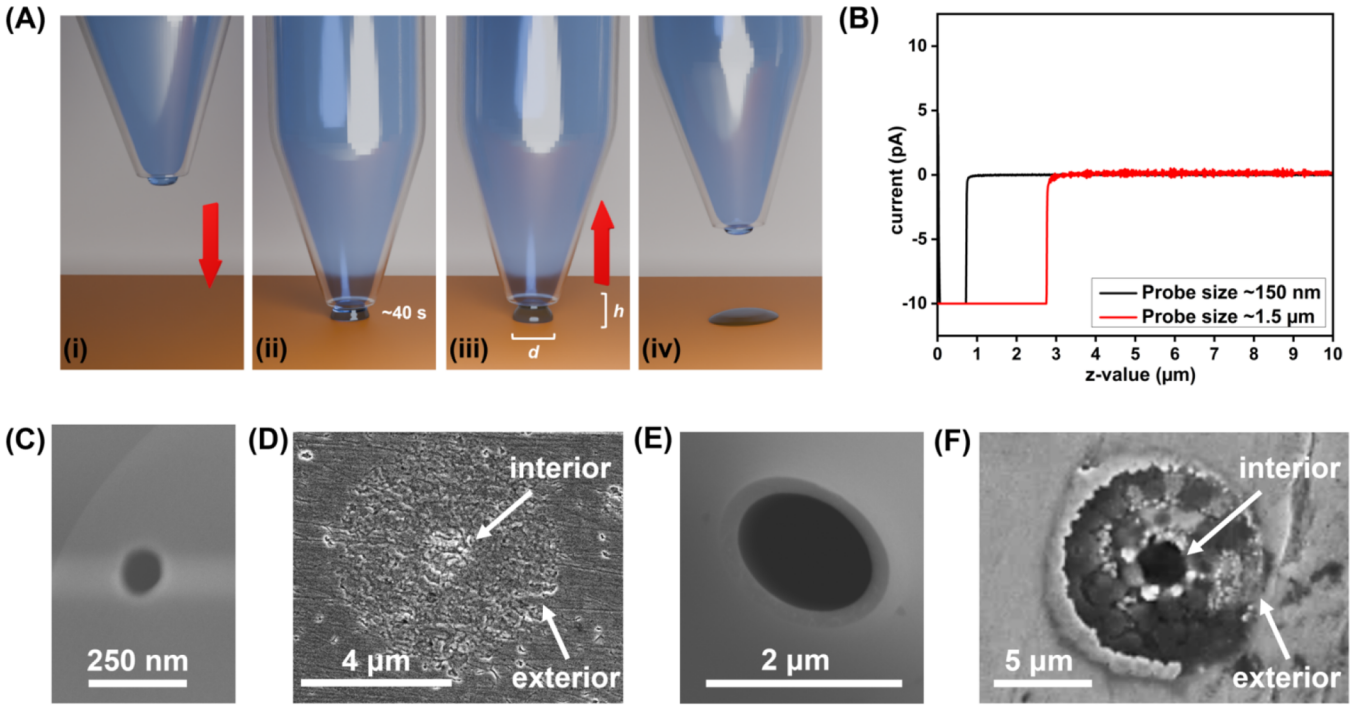

Figure 1. (A) Schematic illustrating the steps of the SECCM experiment: (i) approach, (ii) landing and OCP measurement, (iii) retraction curve, where *d* represents the droplet contact diameter and *h* the droplet stretch distance before detachment, and (iv) complete detachment followed by droplet spreading. (B) Graph showing the current measured as a function of micropipet and nanopipet displacement. (C) SEM image of the nanopipet tip opening and its corresponding (D) SEM image of the droplet footprint, highlighting the interior and exterior regions observed. (E) SEM image of the micropipet tip opening and its corresponding (F) SEM image of the droplet footprint, highlighting the interior and exterior regions observed.

It is known that air-formed surface films such as oxides and adventitious carbon alter the surface energy of a material, hence affecting its wettability. When the Cu sample was exposed to the lab atmosphere, such films grew and the contact angle increased, suggesting a more hydrophobic surface (Figure S1A). Therefore, all the samples were left under ambient conditions for at least 1 day after polishing to form a stable oxide film and to avoid high wetting during measurements as shown in Figure S1B.

2.3. SECCM Probe Fabrication

Borosilicate capillaries from Sutter Instrument (Novato, CA., USA) with dimensions of O.D. = 1.2 mm, I.D. = 0.69 mm, and 10 cm length were pulled using a Sutter Instrument P-2000 laser-based pipet puller (Novato, CA, USA) to provide two nearly identical single barrel micropipets with diameters of approximately 1.5 μm (as determined using FE-SEM) with the following pulling parameters: Line 1: HEAT 350, FIL 4, VEL 25, DEL 200, PUL-; Line 2: HEAT 350, FIL 3, VEL 25, DEL 200, PUL 60. The nanopipets were pulled from Quartz capillaries from Sutter Instrument (Novato, CA., USA) with dimensions O.D.: 1.0 mm, 0.70 mm, and 7.5 cm length, using the same P-2000 laser pipet puller with pulling parameters HEAT 490, FIL 1, VEL 30, DEL 145, PULL 175.[39] The pipet apertures for the nanopipets were approximately 150 nm as determined using FE-SEM. For the silanized experiments, the outer walls of the 1.5 μm pipets were silanized by immersing the tip of the pipet in dichlorodimethylsilane. To prevent the solution from entering inside the pipet tip, an argon flow was provided.

The pipets were filled with a 0.1 M HNO_3 electrolyte (using a MicroFil flexible needle with dimensions O.D.: 350 μm, I.D.: 250 μm, and 67 mm length) that formed the droplet cell at the tip of the pipets. The low vapor pressure of nitric acid makes it a convenient electrolyte for SECCM measurements, as it helps prevent the rapid evaporation of droplets. Additionally, at the selected concentration, the nitric acid solution exhibits relatively low solution resistance, which minimizes the *iR* drop.[18,40,41] The maximum ohmic drop calculated based on the limiting current and solution resistance was 0.16 mV, which is relatively small and within the error of the OCP measurements carried out (full calculation can be found in the Supporting Information). This enables long-term corrosion electrochemical measurements to be performed in air. Ag/AgCl wire was used as the quasi-reference counter electrode (QRCE) and was inserted into the pipet containing the electrolyte. The Ag/AgCl wires were prepared by oxidizing the Ag wire in bleach and rinsing them with ultrapure water. The Ag/AgCl QRCE potential was measured against a commercial saturated calomel electrode (SCE) in 0.1 M HNO_3 solution. The potential was recorded before and after the experiment and did not change more than 3 mV, indicating the stability of the Ag/AgCl QRCE during the experiments (Figure S2).

2.4. SECCM Setup and Measurements

The SECCM measurements were performed by using an ELP1 electrochemical probe scanner and a PG 618 USB Bipotentiostat from HEKA Elektronik (Reutlingen, Germany) enclosed inside a Faraday cage to reduce electrical noise. The measurements were performed using a two-electrode setup: using the Cu sample as the working electrode (WE) and the Ag/AgCl as the QRCE. The positioning system and sample were mounted on an antivibration table. During the micropipet approach toward the substrate, a value of E_{appr} = −250 mV vs QRCE was applied to the WE to avoid Cu oxidation, and a current threshold of 2 pA was selected to signal the discontinuation of movement once the meniscus contacted the WE. The micropipet was moved in the *z*-direction at a rate of −1 μm/s. Then, an open-circuit potential (OCP) measurement was recorded for 40 s at each landing spot. Once completed, the OCP potential was applied to the WE and the micropipet was retraced from the surface as the current was recorded with respect to the *z*-position. All data processing was carried out using MATLAB (R2024b, Mathworks, U.S.A). Statistical analysis was done using OriginPro 2023b (64-bit) SR1.

2.5. Contact Angle Goniometry

The contact angle (CA) measurements were performed using a Krüss DSA30E Drop Shape Analyzer (Hamburg, Germany) goniometer

https://doi.org/10.1021/acsmeasuresciau.4c00042
ACS Meas. Sci. Au 2025, 5, 178−188

equipped with a microsyringe system. Using 0.1 M HNO_3 as the solution of interest, droplets of 0.4 μL were dispensed from a stainless-steel microsyringe (1.8 mm outer diameter). CA measurements were carried out on 1-day exposed wrought Cu samples to represent the surface energy of samples that were used for SECCM measurements at least three times. The average value and related error at a 95% confidence interval were reported. To simulate the setup required for SECCM electrochemical measurements, the needle was in contact with the droplet for 10 s before being elevated. The droplet completely evaporated from the sample's surface after 4 min.

2.6. Surface Analysis

Upon completion of the electrochemical measurements, the droplet footprint diameters, resulting from either electrolyte residue or corrosion products during the SECCM measurements, were examined using a Leica Microsystems GmbH DVM6 digital microscope (Wetzlar, Germany) and their size and the pipet diameter were analyzed by either a Hitachi SU3900 variable pressure scanning electron microscopy (SEM, accelerating voltage of 15 kV, Hitachi, Ltd., Chiyoda City, Tokyo, Japan) coupled with an Oxford ULTIM MAX 65 SDD X-ray detector for energy-dispersive X-ray spectroscopy (EDX), or using a Hitachi SU8230 Regulus ultrahigh-resolution field emission scanning electron microscope (FE-SEM, accelerating voltage of 5 kV, Hitachi, Ltd., Chiyoda City, Tokyo, Japan) combined with a Bruker X-Flash FQ5060 Annular Flat-Quad SSD X-ray detector for EDX. The depth of corrosion inside the droplet footprints was analyzed using a Zeiss LSM800 Confocal Laser Scanning Microscope (CLSM, Carl Zeiss, Germany). The droplet footprint images, captured using SEM/FE-SEM, were analyzed to determine their dimensions. This analysis was conducted using ImageJ software (version 1.54j), where the diameters of the droplet footprints were manually measured.

3. RESULTS AND DISCUSSION

3.1. Retraction Curves to Estimate Droplet Size

The steps involved in the SECCM measurements are shown in Figure 1A. First, the freely hanging droplet/meniscus approaches the substrate (i) while a bias of −62 mV vs SCE is applied to the Cu working electrode (WE).

This potential was chosen because it is more negative than the open circuit potential (OCP) of Cu when exposed to 0.1 M HNO_3 (−12 mV vs SCE), as measured in macroscale measurements performed prior to the SECCM measurements (Figure S3). Once the meniscus contacts the WE, the current response is measured, and the pipet movement is halted. Then, the OCP of the Cu inside of the droplet in contact with the substrate is measured for 40 s (ii) until it has reached an approximate steady state (Figure S4). Upon completion of the OCP measurement, the pipet is retracted from the substrate at a retraction rate of 1 μm/s, while the current is recorded as a function of the pipet's z-position (iii) to result in a retraction curve measurement (Figure 1B). The potential applied during the retraction curve is the last OCP value measured during the (ii) step, and hence, a small current is measured due to small deviations from this value. A tensile stress is applied to the droplet during this step. Finally, the meniscus of the pipet breaks contact with the WE and the electrical connection is severed (iv), where complete detachment is signified by the drop in the current to zero.

Typically, retraction curves are used in SECCM to verify that the electrical connection has been terminated before moving the pipet in the x−y plane.[42] However, there appears to be a correlation with the droplet detachment distance measured by retraction curves (Figure 1B) and the interior droplet footprint diameter of the wetted area on the substrate measured *ex situ* while using a nanopipet (Figures 1 C&D) or a micropipet (Figure 1E,F). During step (iii), the droplet is stretched in the z-direction but keeps contact with the surface due to its surface tension. Therefore, a current is measured as the pipet is retracted from the substrate. Once the surface tension is broken, the current sharply reaches zero. Using a micropipet with a diameter of 1.5 ± 0.1 μm, the droplet contact diameter was estimated to be 2.8 μm by measuring the z-direction distance at which the current reaches zero in the retraction curves in Figure 1B (red plot). This estimation closely aligns with the interior droplet footprint diameter measured *ex situ* by SEM, which was 2.7 μm (as shown in Figure 1F).

In the case of a nanopipet with a diameter of 145 ± 3 nm, the droplet contact diameter was estimated to be 0.8 μm by measuring the z-direction distance at which the current reaches zero in the retraction curves in Figure 1B (black plot). This estimation closely aligns with the interior droplet footprint diameter measured *ex situ* by SEM, which was 1.0 μm (as shown in Figure 1D). Additional examples comparing retraction curves to SEM measurements can be found in Figure S6. These results suggest that it is possible to estimate the droplet contact diameter *in situ* during the SECCM measurements.

It should be noted that the current plateau in Figure 1B is due to signal overload caused by using a current range of ±10 pA. Employing higher current ranges in the retraction curves leads to increased background noise and altered droplet footprint morphology, as shown in Figure S5. This is likely caused by additional corrosion induced by the higher current during the polarization applied to the retraction curves. Therefore, minimizing the current range during retraction curves, especially at polarization values closer to the OCP, is an effective strategy to reduce additional corrosion during measurements. Additionally, the slow ring-down to the current baseline after droplet detachment may be attributed to charging of the pipet. However, this effect does not affect the estimation of the droplet detachment distance, which is determined by the sharp current decay rather than the slower ring-down decay.

Two assumptions are made when using retraction curves to estimate the droplet size. First, the droplet is approximated as a spherical cap, simplifying the calculation of its surface area. This assumption is based on the liquid's natural tendency to minimize surface energy, leading to a near-spherical meniscus shape. Additionally, due to the small droplet size, gravity has a negligible effect on the shape, with surface tension being the dominant factor. In SECCM, the droplet size is in the picoliter range, which may be too small to cause significant spreading during retraction. Due to the accuracy of the retraction curves when compared to the *ex situ* SEM images of the interior droplet footprint diameters, spreading is thought to be observed only after the droplet has fully detached from the pipet. This is attributed to the surface's hydrophilicity, as verified through contact angle measurements (Section 3.2). Therefore, the diameter (d) of the droplet contact is considered to be equal to the maximum stretch distance (h) observed during the detachment process, which is the second assumption. This assumption may be modified depending on the surface tension created with different solvents and substrates analyzed by using SECCM. For instance, these assumptions may not be suitable for highly hydrophilic or heterogeneously wetted areas of contact. Further investigation of the applicability of retraction curves for droplet size

https://doi.org/10.1021/acsmeasuresciau.4c00042
ACS Meas. Sci. Au 2025, 5, 178−188

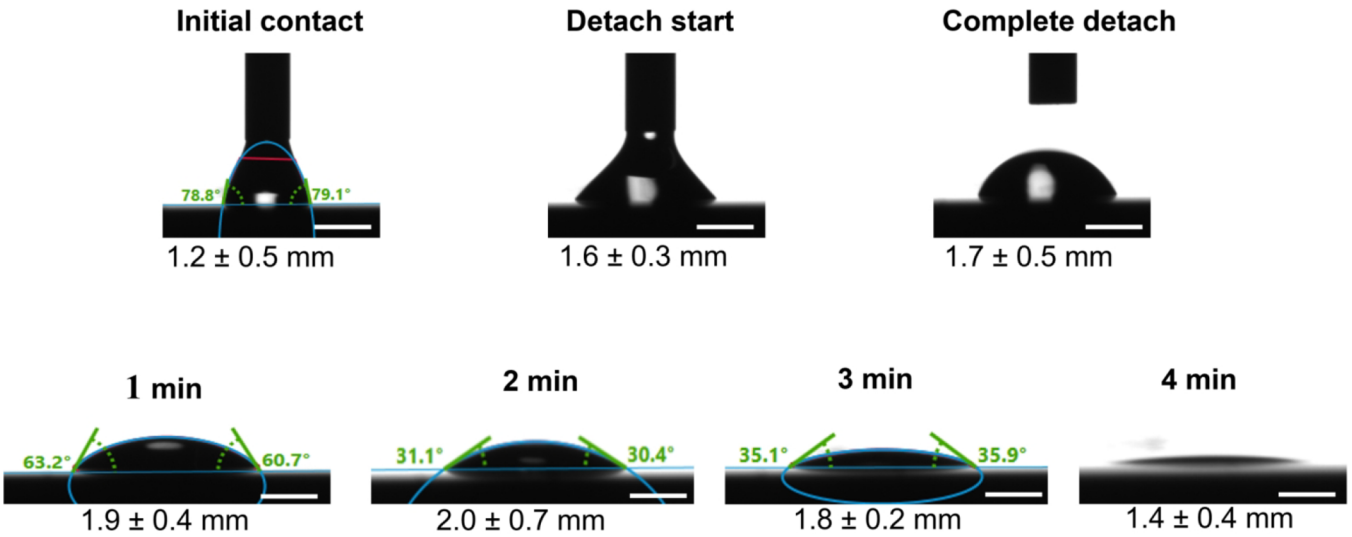

Figure 2. Mesoscale goniometer measurements of the contact angle of 0.1 M HNO_3 on Cu. The variation in the size of the droplet on an aged wrought Cu sample was monitored during initial contact and detachment. The droplet size increased during dispensing needle retraction until it completely evaporated after 4 min. The scale bar represents 0.5 mm.

estimations should be performed for such materials. Also, in SECCM, the impact of mass transport is minimized due to the localized nature of the technique and the restricted diffusion layer within the small droplet at the pipet tip. Even when mass transport limitations occur, the retraction curves are primarily governed by the physical contact of droplets on the surface, rather than relying on mass transport regime, which increases the method's transferability to other electrochemical systems. This method of droplet size determination allows for the *in situ* (i.e., the ability to estimate the droplet contact diameter simultaneously during the SECCM measurement) estimation of the droplet's surface area at each point of measurement. This is a significant advantage, as it provides real-time data on the droplet's behavior and interaction with the substrate without the need for time-consuming *ex situ* analysis of each droplet footprint. It is also noted that the pipet sizes determined from SEM (1.5 ± 0.1 μm for the micropipet and 145 ± 3 nm for the nanopipet) are significantly smaller than the droplet footprint diameters measured via SEM. This suggests that if the working electrode's surface area is estimated solely based on the pipet size, it may lead to an overestimation of corrosion rates when performing polarization measurements during SECCM. This highlights the importance of considering both the pipet size and the droplet footprint diameter in SECCM experiments to ensure reliable and accurate estimation of corrosion rates.

Upon *ex situ* analysis of the droplet footprints diameter using SEM, it was observed that there were two wetted regions: an interior and exterior diameter (Figures 1D and 1F), indicative of droplet spreading. While the interior droplet footprint diameter correlated well with the retraction curves, the exterior droplet footprint diameter was much larger, at ∼5 and 11 μm in Figures 1D and 1F, respectively. To accurately measure the working electrode's surface area, it is crucial to know whether the exterior regions stem from droplet spreading during a SECCM measurement, causing a dynamic surface area of the working electrode, or post SECCM measurement once the pipet has been retracted from the substrate.

3.2. Visualization of Droplet Spreading

The similarity in the sizes between the measurements of the droplet contact diameter from the retraction curves and the interior region of the droplet footprint suggests that the droplets spread once the pipet is retraced from the surface.

To investigate this droplet spreading phenomenon, a visualization of the droplets' contact angles during retraction was carried out at the mesoscale using a goniometer as a proxy experiment to SECCM. Using 0.1 M HNO_3 as the solution, the contact angles measured, as shown in Figure 2, were consistently less than 90°, indicating that the Cu surface was hydrophilic and could promote the spreading of the droplet during SECCM measurements.

When the dispensing needle was stagnant, the contact angle did not change, and there were no visible changes in droplet size. Further analysis of droplet dynamics during retraction showed that immediately after detachment, the droplet was considerably larger than its initial size upon contact with the surface. This increase in size can be attributed to the surface's hydrophilic properties, which encourage the spreading of the droplet once the surface tension is broken between the droplet and the dispensing needle. Over time, the droplet continued to spread until evaporation caused a shrinkage.

It is important to recognize that mesoscale goniometer measurements were conducted to visualize wetting and spreading behavior. These measurements provide insights into contact angle dynamics but may not fully capture the intricacies of the SECCM environment. Specifically, the application of pressure to the syringe plunger to dispense the droplet results in a spherical droplet geometry as shown in Figure 2. In contrast, no such pressure is applied to the micropipet in SECCM measurements. The droplet hangs freely from the tip of the pipet due to the gravitational force and capillary action, resulting in a meniscus of electrolyte. Furthermore, the droplet size is much larger in the goniometer measurements, whereas in SECCM, the droplets are on the order of picoliters.[43] The size and pressure used in the mesoscale measurements may be the reason why spreading appears to occur during retraction in Figure 2, whereas the accuracy of the retraction curves suggests that spreading occurs

https://doi.org/10.1021/acsmeasuresciau.4c00042
ACS Meas. Sci. Au 2025, 5, 178−188

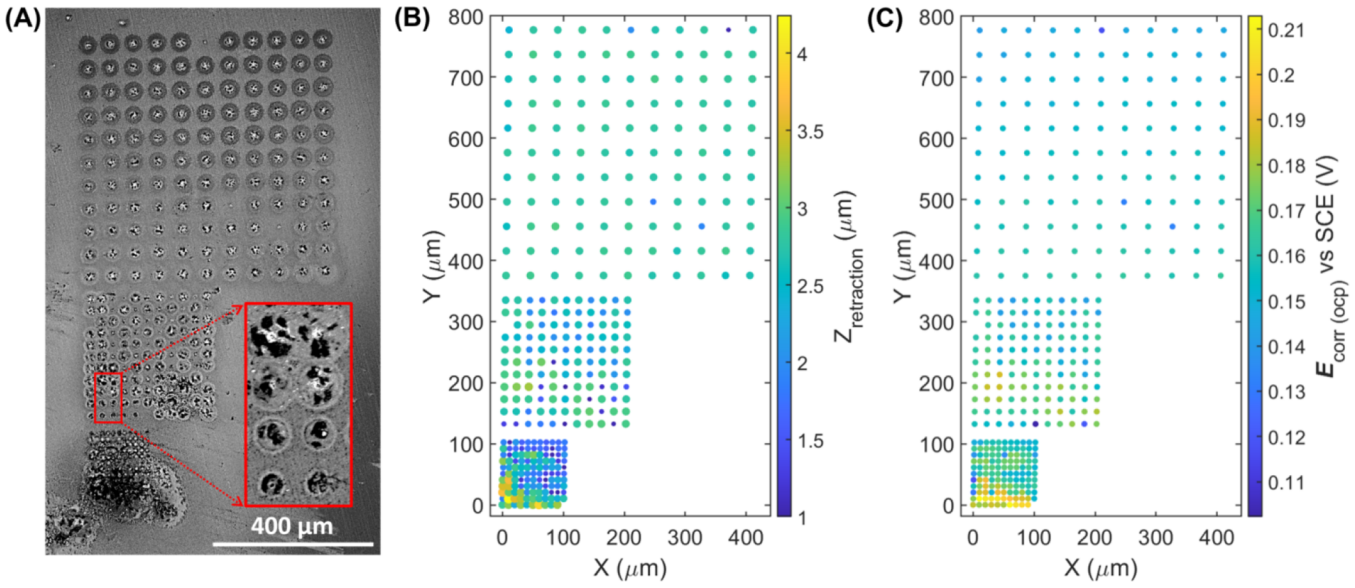

Figure 3. Effect of landing separation distance between SECCM measurements. (A) SEM image showing three different matrices measured at separation distances of 8 μm (bottom), 16 μm (middle), and 24 μm (top). The point (0,0) at the bottom-left marks the starting point of the measurements. (B) Diameter of each droplet contact inferred from the retraction curve. The different sizes of footprints are proportional but not to scale. (C) Open circuit potential (OCP) measured at each landing site, with the displayed value representing the average of the last 5% of the data.

post pipet detachment. Despite these differences, the use of a goniometer is justified as a preliminary step to visualize wetting interactions on the Cu surface during pipet detachment, which suggest that spreading occurs during or shortly after pipet retraction.

The spreading of the droplet has significant implications for determining the true surface area of the working electrode in SECCM measurements. Extrapolating the exterior diameter of the droplet footprint as the size of the working electrode may lead to inaccuracies in the interpretation of electrochemical data when normalizing the current, where the current density may be estimated to be much smaller than its true value.

3.3. Effect of Landing Separation and Pipet Silanization on SECCM Measurements

Knowing that the droplets spread post retraction of the pipet, the chosen separation distance between two landing regions is one of the critical parameters for such SECCM measurements. The landing separation was varied for three SECCM matrices: 8 μm, 16 μm, and 24 μm (Figure 3). It was observed that if the separation distance was too small as in the case of the first and second matrices, the droplets could overlap with nearby scanning sites covered with corrosion products, which may alter the surface wettability and hence influence the droplet spreading behavior, which eventually leads to formation of a thick layer of corrosion products on the surface (Figure 3A). As observed in the working electrode diameter map estimated by retraction curves (or "retraction maps") presented in Figure 3B, when the droplet overlapped with previous scanned areas, the droplet size was substantially larger and inconsistent, as confirmed by the SEM image *ex situ*. Furthermore, the retraction map for the well-separated droplet matrix (24 μm separation distance) exhibited a more uniform and smaller size distribution, which also aligns well with the SEM image.

The separation distance is also an important parameter, as it can affect the corrosion potentials extracted during OCP measurements. As illustrated in Figure 3C, the corrosion potential was significantly higher in the bottom matrix (separation distance 8 μm), where droplet overlapping with previous scanned areas was observed, compared to the top matrix (separation distance 24 μm), where the droplets were well separated The observed nonuniformity in corrosion potentials in the first matrix can be attributed to the overlapping of droplets with previously scanned areas, which have already undergone corrosion during electrochemical measurements. These precorroded areas may have a different concentration of Cu ions in solution, contributing to a higher corrosion potential. In addition, the larger droplet may also portray a different diffusion profile, enabling a higher concentration of oxygen, which may increase the corrosion potential. Conversely, the top matrix measured using a separation distance of 24 μm exhibited more uniform corrosion potentials due to a decreased likelihood of such an overlap as they are well separated from each other.

The confinement and stability of the droplet in SECCM can be effectively controlled by modifying the surface properties of the pipets, specifically through functionalizing the outer walls via silanization.[15,44] Therefore, the effect of using a silanized pipet on the spreading and size of the droplets measured from retraction curves was investigated using a pipet aperture of 1.5 μm. As shown in Figure S9B, the droplet sizes estimated from the retraction curves did not exhibit significant variation but were still larger than the pipet aperture. Furthermore, as seen in the optical image (Figure S9A), droplet spreading was still observed after pipet retraction, indicated by the exterior region of the droplet footprints. This confirms that spreading arises from the hydrophilic nature of the Cu substrate and that it occurs after pipet detachment. Nonetheless, the calibration plot (Figure S9C) shows a strong correlation between the interior droplet footprint diameter measured through microscopy and the droplet contact diameter measured from retraction curves. This consistency confirms that the retraction curves provide a reliable and accurate *in situ* method for estimating the surface area of the working electrode, even when silanized pipets are used.

https://doi.org/10.1021/acsmeasuresciau.4c00042
ACS Meas. Sci. Au 2025, 5, 178−188

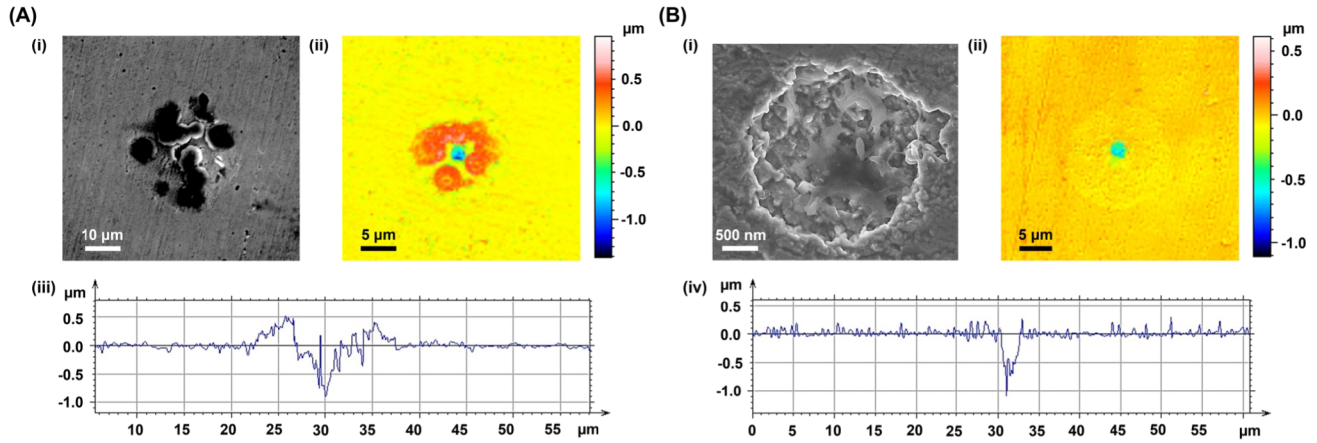

Figure 4. (A) Droplet footprints covered with corrosion products: (i) SEM image, (ii) profilometry image, and (iii) profilogram. (B) Droplet footprint after cleaning and removing the corrosion products: (i) SEM image, (ii) profilometry image, and (iii) profilogram. Profilograms were obtained by crossing the center of the footprint.

3.4. Effect of Cleaning Corrosion Products Post SECCM Measurements

Sometimes, the droplet footprints are covered with the residues of the electrolyte and/or the corrosion products, which can eventually mask the true surface area of the working electrode (Figure 4A). Therefore, a cleaning procedure was necessary to remove these products to observe the true region analyzed. Yet, it is interesting to observe the corrosion products and damage pattern post SECCM measurements prior to cleaning the substrate. As illustrated in Figure S7, the corrosion product was rich in Cu, O, and N species. It is clear that Cu oxidation occurred in the center of the droplet, whereas corrosion products tended to deposit around the perimeter of the droplet, probably in the cathodic regions due to the higher ingress of oxygen. The Cu ions diffuse from the center (pit) to the surface and may react with nitric acid, forming nitrogen-containing corrosion product species around the hole. This is shown in the profilometry images in Figure 4A(ii), where an increase in height is shown on the exterior regions of the droplet footprint and a pitlike structure is seen inside of the footprint.

To accurately determine the working electrode surface area during SECCM to avoid underestimation of the corrosion rate (which may occur when using the exterior droplet footprint as the electrode's surface area), it is essential to clean the surface post experiment. After surface cleaning with a dilute HCl solution (1:2 ratio of HCl:water, from a modified ASTM standard),[45] the droplet footprint morphology was observed via FE-SEM (Figure 4B(i)), which showed a surface free of corrosion products. This is evident by the EDX elemental analysis (Figure S8), which indicated a significantly reduced nitrogen and oxygen content. Additionally, the profilometry maps illustrated the removal of the protruding regions, confirming the absence of corrosion products surrounding the pit formed during SECCM measurements at OCP.

Finally, the diameters of the interior droplet footprints as observed from SEM were compared to the droplet contact sizes estimated by retraction curves. Based on the calibration curve shown in Figure 5 that portrays relatively good linearity, we demonstrate that retraction curves provide a reliable *in situ* method for estimating the droplet contact diameter. It is evident that the variability in the droplet size obtained from the SEM images (*x*-axis) is larger than the data spread in the estimated droplet size from the retraction curves (*y*-axis), especially for the measurements performed using a nanopipet. This may be due to droplet spreading after pipet detachment, prior to droplet evaporation, where the corrosive electrolyte remains on the substrate and can continue to oxidize the metal post OCP measurement.

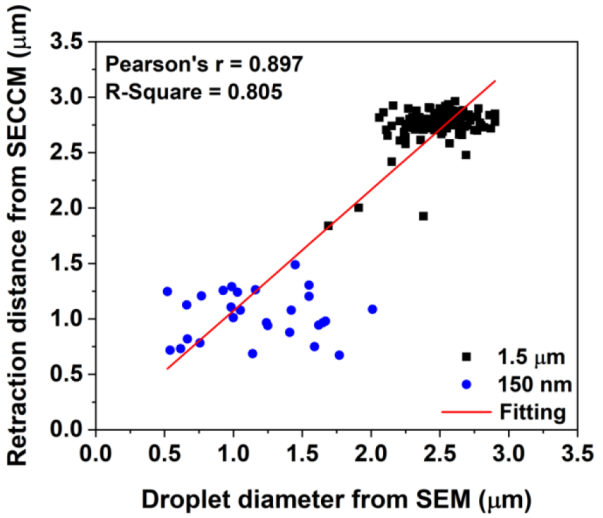

Figure 5. Calibration curve for 1.5 μm (from landing separation experiment) and 150 nm (from retraction rate experiment) pipet apertures, comparing the diameters of the interior droplet footprints measured by SEM (*x*-axis) and diameter of droplet contact by retraction curves (*y*-axis). The data corresponds to 121 points for 1.5 μm pipet and 28 points for 150 nm pipet.

3.5. Effect of the Retraction Rate on the Wetted Area

Considering the influence of the retraction rate on the retraction curves may be an important experimental factor when using such a method to estimate the wetted area *in situ* and thus was systematically investigated.

SECCM measurements were performed using a separation distance between two points of 30 μm, and the retraction rates of the first (bottom), second (middle), and third (top) matrices were chosen to be 1, 5, and 10 μm/s based on the size of the micropipet used, as shown in Figure 6A. As observed, the higher the retraction rate, the more the spreading due to

https://doi.org/10.1021/acsmeasuresciau.4c00042
ACS Meas. Sci. Au 2025, 5, 178−188

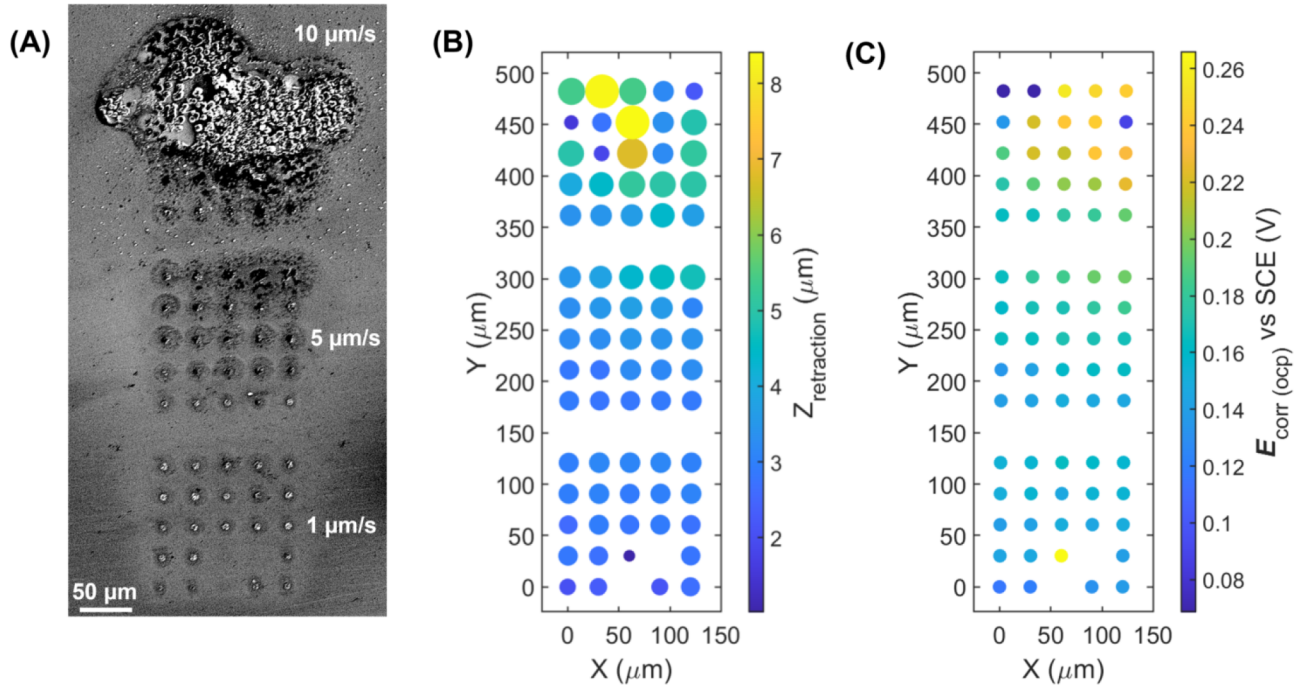

Figure 6. (A) FE-SEM image showing the effect of the retraction rate (using 1.5 μm micropipet) on the size of the droplet footprints with its corresponding retraction rates for each matrix mapped.. (B) Diameter of each droplet contact, inferred from the retraction curve. The different sizes of footprint sizes are proportional but not to scale. (C) Corrosion potential map obtained from OCP measurements, where the displayed value represents the average of the last 5% of the data. Some landing regions were unsuccessful, resulting in missing points in the bottom matrix. The point (0,0) at the bottom-left marks the starting point of the measurements.

overlapping of the droplets with previously scanned areas covered with corrosion products across the surface.

This also correlates well with the size of the droplets from the retraction maps, as seen in Figure 6B, where the droplets' contact diameters are much larger at faster retraction rates compared to the diameters at slower retraction rates. This may be due to the high acceleration of the pipet's upward motion, which induces elongational deformation of the droplet at the pipet tip and a pulling force on the solution inside of the pipet.

As the pipet ascends, the solution experiences an increase in tensile force along the *z*-axis, leading to an expulsion and a subsequent increase in droplet contact diameter. By analyzing the interplay between retraction rate and droplet deformation, the size of the droplet can be controlled, ensuring more accurate and reproducible results during the measurements.

It was hypothesized that the retraction rate should be approximately equivalent to one pipet diameter per second to minimize droplet spreading on the surface. For instance, with a pipet diameter of 1.5 μm, a retraction rate of 1 μm/s was chosen to produce droplet contact diameter with less spreading and deformation. Lower retraction rates, while might reduce spreading, would significantly increase the overall experiment time. At higher retraction rates, such as 5 and 10 μm/s, an increase in droplet diameter is observed due to an overlap with previous scanned areas, which may have been caused by an increase in wettability due to corrosion products formed at previous landing sites. As a result, inaccurate measurements of corrosion potentials are recorded, as depicted in Figure 6C.

Similar results were observed when a 150 nm pipet was employed to investigate the effect of the retraction rate on the wetted area. While using higher retraction rates of 5 and 10 μm/s, there was an increase in the droplet diameter as seen in Figure S10A, which correlated well with the size of the droplets measured during the retraction maps in Figure S10B. This demonstrates that retraction curves provide a reliable *in situ* method for estimating the droplet contact diameter, as confirmed by the calibration curve in Figure 5, which compares the diameters estimated by SEM and retraction curves.

This overlap results in significantly elevated corrosion potentials, indicating that the retraction rate is a critical experimental parameter in SECCM. It can influence electrochemical measurements by affecting the spatial resolution and the accuracy of the data obtained. Therefore, the careful optimization of the retraction rate is essential during SECCM measurements.

As previously discussed, it is crucial to clean the surface post experiment because the presence of corrosion products or residues from the electrolyte obscures the droplet footprints and complicates the *ex situ* estimation of the actual interior droplet footprint diameter. Once the surface was cleaned, the interior droplet footprints' diameters measured from SEM aligned well with those determined *in situ* using retraction curves as shown in Table 1. The average value for three scanning points for each retraction rate and related error at a

Table 1. Comparative Analysis of Droplet Contact Diameter Using Retraction Curves with a Pipet Size of Approximately 1.5 μm and Interior Droplet Footprint Diameter Microscopy Methods (the Error Is the 95% Confidence Interval)

retraction rates	1 μm/s	5 μm/s	10 μm/s
retraction curve (*in situ*)	3.1 ± 0.2 μm	4.5 ± 0.4 μm	3.9 ± 1.1 μm
microscopy methods (*ex situ*)	2.8 ± 0.2 μm	4.3 ± 0.1 μm	3.7 ± 0.4 μm

https://doi.org/10.1021/acsmeasuresciau.4c00042
ACS Meas. Sci. Au 2025, 5, 178−188

95% confidence interval are reported. These results demonstrate the reliability of the retraction curves for estimating the droplet contact diameter *in situ* at different retraction rates.

We note that if the separation distance is large enough to avoid the droplet overlap, the retraction rate should not affect the wetted area during an individual electrochemical measurement since spreading is only induced during pipet retraction (as seen for the first measurements performed at the beginning of each matrix in Figure 6C). However, a retraction rate analysis should be performed for other systems to validate this assumption, as we have clearly shown that when droplets overlap due to post retraction spreading and an inefficient landing separation distance is chosen, their size will increase.

For systems such as the one studied, where the oxide can be removed readily from the copper surface post experiment, to allow for comparison of *in situ* and *ex situ* results as shown in Figure 5, the correlation between methods validates the retraction curve method. However, to extend the applicability of the retraction curve method beyond this somewhat ideal system demonstrates additional promise. The elimination of the need to remove the oxide to obtain the surface area measurement inherently lowers the possibility of error that will occur from incomplete or overly aggressive methods to remove oxides that are more tightly bound to the surface (i.e., for passive metals such as stainless steel, titanium, etc.). Thus, the wider applicability of the technique may be realized in other systems, which will be studied in the near future.

This study holds significant importance beyond corrosion analysis, particularly in areas such as electrocatalysis[46] and energy storage.[47] In these fields, the catalytic efficiency is evaluated by the current density. During SECCM measurements of such materials, accurately estimating the contact area of the meniscus is crucial for determining the activity of the material. The use of retraction curves to estimate the true surface area analyzed may enable more precise evaluations of these materials' local catalytic or electrochemical performances using SECCM.

4. CONCLUSIONS

This study introduces a novel and quick methodology for quantifying the working electrode surface area during SECCM measurements, aimed at improving the accuracy of the localized corrosion rate analysis. Our findings demonstrate that retraction curves are a promising tool for estimating the surface area *in situ*, thus preventing over/under estimations typically encountered during SECCM measurements. This work also highlights the necessity of post experiment surface cleaning to remove corrosion products or electrolyte residues that can obscure the true size of droplet footprints, thereby enabling accurate *ex situ* surface area determination. By using retraction curves to estimate the wetted area, researchers can avoid time-consuming *ex situ* image analysis. Furthermore, it was observed that the exterior droplet footprint diameter overestimates the working electrode surface area due to droplet spreading during pipet detachment. However, the estimated surface area from the interior droplet footprint diameter and retraction curves are within good agreement with each other, highlighting that the pipet aperture may not accurately represent the true area as it may lead to overestimation of corrosion rates. Therefore, these findings provide a powerful tool for obtaining a statistical analysis of working electrode surface area for accurate corrosion rate analysis.

Future work will involve conducting polarization electrochemical measurements using SECCM to statistically analyze local corrosion rates and exploring the Cu coating's local electrochemical reactivity. This analysis will be correlated to the microstructure of copper materials using complementary microscopy methods. Ultimately, the relationship between the electrochemical responses of individual microstructural features and the surface-averaged responses of the macroscopic surface will be investigated with accuracy, providing a comprehensive understanding of the localized copper corrosion phenomena.

■ ASSOCIATED CONTENT

Supporting Information

The Supporting Information is available free of charge at https://pubs.acs.org/doi/10.1021/acsmeasuresciau.4c00042.

Experimental section for bulk electrochemistry and iR drop calculation are included, as well as additional figures including: a graph showing the effect of aging time on contact angle and microscope image of the droplet spreading on a freshly polished sample, graph showing the stability of the Ag/AgCl QRCE, macroscale OCP data of copper in nitric acid and OCP during SECCM electrochemical measurements, effect of the current range on retraction curves, SEM image of a 4 × 4 matrix showing the diameter (interior) of each droplet footprint after cleaning and their corresponding retraction curves, EDX elemental analysis of a droplet footprint covered with corrosion products and a cleaned droplet footprint, impact of using a silanized pipet on SECCM retraction curve measurements, and confocal image showing the effect of the retraction rate (using 150 nm nanopipet) on the size of the droplet footprints, diameter of each droplet contact, inferred from the retraction curve, and corrosion potential map obtained from OCP measurements (PDF)

■ AUTHOR INFORMATION

Corresponding Author

Samantha Michelle Gateman − *Department of Chemistry, The University of Western Ontario, London, Ontario N6A 5B7, Canada; Surface Science Western, The University of Western Ontario, London, Ontario N6G 0J3, Canada;* orcid.org/0000-0002-3889-9926; Email: samantha.gateman@uwo.ca

Authors

Nishtha Saxena − *Department of Chemistry, The University of Western Ontario, London, Ontario N6A 5B7, Canada*

Emmanuel Mena-Morcillo − *Department of Chemistry, The University of Western Ontario, London, Ontario N6A 5B7, Canada;* orcid.org/0000-0002-3193-0003

Mia Tripp − *Department of Chemistry, The University of Western Ontario, London, Ontario N6A 5B7, Canada*

Peter George Keech − *Nuclear Waste Management Organization, Toronto, Ontario M4T 2S3, Canada*

Mehran Behazin − *Nuclear Waste Management Organization, Toronto, Ontario M4T 2S3, Canada*

Complete contact information is available at: https://pubs.acs.org/10.1021/acsmeasuresciau.4c00042

Author Contributions

CRediT: **Nishtha Saxena** data curation, formal analysis, investigation, writing - original draft; **Emmanuel Mena-Morcillo** data curation, formal analysis, investigation, methodology, writing - review & editing; **Mia Tripp** data curation, formal analysis; **Peter George Keech** project administration, resources, validation, writing - review & editing; **Mehran Behazin** project administration, resources, writing - review & editing; **Samantha Michelle Gateman** conceptualization, funding acquisition, project administration, resources, supervision, writing - review & editing.

Funding

This work was financially supported by an NSERC Alliance Grant (ALLRP 578485) and the Nuclear Waste Management Organization (NWMO).

Notes

The authors declare no competing financial interest.

■ ACKNOWLEDGMENTS

Authors thank research scientists at Surface Science Western for their assistance with SEM-EDX, FE-SEM, and CLSM training; Reza Moshrefi for preparing Figure 1A; and Jingpeng (Frank) Wang from HEKA Electronik GmbH for the technical assistance.

■ REFERENCES

(1) Ralston, K. D.; Birbilis, N. Effect of Grain Size on Corrosion: A Review. *Corrosion* **2010**, *66* (7), No. 075005.
(2) Daviddi, E.; Shkirskiy, V.; Kirkman, P. M.; Robin, M. P.; Bentley, C. L.; Unwin, P. R. Nanoscale Electrochemistry in a Copper/Aqueous/Oil Three-Phase System: Surface Structure−Activity-Corrosion Potential Relationships. *Chemical Science* **2021**, *12* (8), 3055−3069.
(3) Yan, J.; Heckman, N. M.; Velasco, L.; Hodge, A. M. Improve Sensitization and Corrosion Resistance of an Al-Mg Alloy by Optimization of Grain Boundaries. *Sci. Rep* **2016**, *6* (1), 26870.
(4) Man, C.; Dong, C.; Xiao, K.; Yu, Q.; Li, X. The Combined Effect of Chemical and Structural Factors on Pitting Corrosion Induced by MnS-(Cr, Mn, Al)O Duplex Inclusions. *Corrosion* **2018**, *74* (3), 312−325.
(5) Dobkowska, A.; Castillo, M. D. H.; Turnbull, J. P.; Ramamurthy, S.; Zagidulin, D.; Moser, D. E.; Behazin, M.; Keech, P. G.; Shoesmith, D. W.; Noël, J. J. A Comparison of the Corrosion Behaviour of Copper Materials in Dilute Nitric Acid. *Corros. Sci.* **2021**, *192*, No. 109778.
(6) Turnbull, J.; Szukalo, R.; Zagidulin, D.; Shoesmith, D. Nitrite Effects on Copper Corrosion in Nitric Acid Solutions. *Corros. Sci.* **2021**, *179*, No. 109147.
(7) Gupta, S. K.; Patil, A. P.; Rathod, R. C.; Tandon, V.; Gupta, A. Characterization of Microstructure, Mechanical and Corrosion Response in AISI 304L and Ti-Stabilized 439 Stainless Steels Weld Joints. *Journal of Manufacturing Processes* **2023**, *101*, 721−736.
(8) Zhang, H.; Xu, J.; Hao, D.; Esmail, O. M. A. O. Microstructure and Mechanical Properties of Laser-Welded Joints between DP590 Dual-Phase Steel and 304 Stainless Steel with Preset Nickel Coating. *Materials* **2023**, *16* (7), 2774.
(9) Pinto, E. M.; Ramos, A. S.; Vieira, M. T.; Brett, C. M. A. A Corrosion Study of Nanocrystalline Copper Thin Films. *Corros. Sci.* **2010**, *52* (12), 3891−3895.
(10) Jadhav, N.; Gelling, V. J. Review—The Use of Localized Electrochemical Techniques for Corrosion Studies. *J. Electrochem. Soc.* **2019**, *166* (11), C3461.
(11) Skaanvik, S. A.; Gateman, S. M. Probing Passivity of Corroding Metals Using Scanning Electrochemical Probe Microscopy. *Electrochemical Science Advances* **2023**, No. e2300014.
(12) Payne, N. A.; Stephens, L. I.; Mauzeroll, J. The Application of Scanning Electrochemical Microscopy to Corrosion Research. *Corrosion* **2017**, *73* (7), 759−780.
(13) Mena-Morcillo, E.; Ebrahimzadeh Pilehrood, A.; Moshrefi, R.; Shafiee, G.; Keech, P. G.; Behazin, M.; Gateman, S. M. Effect of Redox Mediators on Corrosion Behavior and Scanning Electrochemical Microscopy Response. *Anal. Chem.* **2024**, *96* (22), 9122−9131.
(14) Gaudin, L. F.; Wright, I. R.; Harris-Lee, T. R.; Jayamaha, G.; Kang, M.; Bentley, C. L. Five Years of Scanning Electrochemical Cell Microscopy (SECCM): New Insights and Innovations. *Nanoscale* **2024**, *16* (26), 12345−12367.
(15) Jayamaha, G.; Maleki, M.; Bentley, C. L.; Kang, M. Practical Guidelines for the Use of Scanning Electrochemical Cell Microscopy (SECCM). *Analyst* **2024**, *149* (9), 2542−2555.
(16) Suter, T.; Böhni, H. A New Microelectrochemical Method to Study Pit Initiation on Stainless Steels. *Electrochim. Acta* **1997**, *42* (20), 3275−3280.
(17) Böhni, H.; Suter, T.; Schreyer, A. Micro- and Nanotechniques to Study Localized Corrosion. *Electrochim. Acta* **1995**, *40* (10), 1361−1368.
(18) Yule, L. C.; Bentley, C. L.; West, G.; Shollock, B. A.; Unwin, P. R. Scanning Electrochemical Cell Microscopy: A Versatile Method for Highly Localised Corrosion Related Measurements on Metal Surfaces. *Electrochim. Acta* **2019**, *298*, 80−88.
(19) Bentley, C. L.; Kang, M.; Unwin, P. R. Nanoscale Surface Structure−Activity in Electrochemistry and Electrocatalysis. *J. Am. Chem. Soc.* **2019**, *141* (6), 2179−2193.
(20) Li, Y.; Morel, A.; Gallant, D.; Mauzeroll, J. Correlating Corrosion to Surface Grain Orientations of Polycrystalline Aluminum Alloy by Scanning Electrochemical Cell Microscopy. *ACS Appl. Mater. Interfaces* **2022**, *14* (41), 47230−47236.
(21) Wang, Y.; Li, M.; Gordon, E.; Ye, Z.; Ren, H. Nanoscale Colocalized Electrochemical and Structural Mapping of Metal Dissolution Reaction. *Anal. Chem.* **2022**, *94* (25), 9058−9064.
(22) Jayamaha, G.; Tegg, L.; Bentley, C. L.; Kang, M. High Throughput Correlative Electrochemistry-Microscopy Analysis on a Zn−Al Alloy. *ACS Phys. Chem. Au* **2024**, *4*, 375.
(23) Gateman, S. M.; Gharbi, O.; Turmine, M.; Vivier, V. Measuring Changes in Wettability and Surface Area during Micro Droplet Corrosion Measurements. *Electrochim. Acta* **2021**, *399*, No. 139402.
(24) Shamai, R.; Andelman, D.; Berge, B.; Hayes, R. Water, Electricity, and Between··· On Electrowetting and Its Applications. *Soft Matter* **2008**, *4* (1), 38−45.
(25) Yule, L. C. *High Resolution Electrochemical Measurements for Corrosion*. PhD Thesis, University of Warwick, 2019. https://wrap.warwick.ac.uk/157548/ (accessed 2024−07−09).
(26) Aballe, A.; Bethencourt, M.; Botana, F. J.; Marcos, M.; Sánchez-Amaya, J. M. Influence of the Degree of Polishing of Alloy AA 5083 on Its Behaviour against Localised Alkaline Corrosion. *Corros. Sci.* **2004**, *46* (8), 1909−1920.
(27) Gateman, S. M.; Page, K.; Halimi, I.; Nascimento, A. R. C.; Savoie, S.; Schulz, R.; Moreau, C.; Parkin, I. P.; Mauzeroll, J. Corrosion of One-Step Superhydrophobic Stainless-Steel Thermal Spray Coatings. *ACS Appl. Mater. Interfaces* **2020**, *12* (1), 1523−1532.
(28) Gateman, S. M.; Georgescu, N. S.; Kim, M.-K.; Jung, I.-H.; Mauzeroll, J. Efficient Measurement of the Influence of Chemical Composition on Corrosion: Analysis of an Mg-Al Diffusion Couple Using Scanning Micropipette Contact Method. *J. Electrochem. Soc.* **2019**, *166* (16), C624−C630.
(29) Coelho, L. B.; Torres, D.; Bernal, M.; Paldino, G. M.; Bontempi, G.; Ustarroz, J. Probing the Randomness of the Local Current Distributions of 316 L Stainless Steel Corrosion in NaCl Solution. *Corros. Sci.* **2023**, *217*, No. 111104.
(30) Valavanis, D.; Ciocci, P.; Meloni, G. N.; Morris, P.; Lemineur, J.-F.; McPherson, I. J.; Kanoufi, F.; Unwin, P. R. Hybrid Scanning Electrochemical Cell Microscopy-Interference Reflection Microscopy (SECCM-IRM): Tracking Phase Formation on Surfaces in Small Volumes. *Faraday Discuss.* **2022**, *233* (0), 122−148.

(31) *An overview of the Canadian nuclear waste corrosion program - Binns - 2023 - Materials and Corrosion - Wiley Online Library*. https://onlinelibrary.wiley.com/doi/10.1002/maco.202313763 (accessed 2024−07−11).
(32) Widen, H.; Sellin, P. *Performance of the SKB Copper/Steel Canister*; Swedish Nuclear Fuel and Waste Management Co. 0284−3757; Sweden, 1994; p 59.
(33) Hänninen, H.; Forsström, A.; Yagodzinskyy, Y. 11 - Copper Behavior in Geological Nuclear Waste Disposal. In *Nuclear Corrosion*; Ritter, S., Ed.; European Federation of Corrosion (EFC) Series; Woodhead Publishing, 2020; Vol. *69*, pp 391−402. .
(34) *Atlas of Electrochemical Equilibria in Aqueous Solutions*. AMPP Store. https://store.ampp.org/atlas-of-electrochemical-equilibria-in-aqueous-solu (accessed 2024−07−11).
(35) Guo, M. *The Electrochemical and Corrosion Study of Copper for Nuclear Waste Containers Under Deep Geological Disposal Conditions*. Ph.D., The University of Western Ontario (Canada): Canada -- Ontario, CA, 2020. https://www.proquest.com/docview/2714870178/abstract/8D94EDE35EC74653PQ/1 (accessed 2024−07−11).
(36) Morco, R. P.; Joseph, J. M.; Hall, D. S.; Medri, C.; Shoesmith, D. W.; Wren, J. C. Modelling of Radiolytic Production of HNO3 Relevant to Corrosion of a Used Fuel Container in Deep Geologic Repository Environments. *Corros. Eng., Sci. Technol.* **2017**, *52* (1_suppl), 141−147.
(37) Björkbacka, Å.; Johnson, C. M.; Leygraf, C.; Jonsson, M. Radiation Induced Corrosion of Copper in Humid Air and Argon Atmospheres. *J. Electrochem. Soc.* **2017**, *164* (4), C201.
(38) Li, W.; Yu, B.; Tam, J.; Giallonardo, J. D.; Doyle, D.; Poirier, D.; Legoux, J.-G.; Lin, P.; Palumbo, G.; Erb, U. Microstructural Characterization of Copper Coatings in Development for Application to Used Nuclear Fuel Containers. *J. Nucl. Mater.* **2020**, *532*, No. 152039.
(39) Wang, Y.; Li, M.; Ren, H. Interfacial Structure and Energy Determine the Heterogeneity in the Electrochemical Metal Dissolution Activity at Grain Boundary. *Chem. Mater.* **2023**, *35* (11), 4243−4249.
(40) Blount, B.; Juarez, G.; Wang, Y.; Ren, H. iR Drop in Scanning Electrochemical Cell Microscopy. *Faraday Discuss.* **2022**, *233* (0), 149−162.
(41) Birbilis, N.; Padgett, B. N.; Buchheit, R. G. Limitations in Microelectrochemical Capillary Cell Testing and Transformation of Electrochemical Transients for Acquisition of Microcell Impedance Data. *Electrochim. Acta* **2005**, *50* (16), 3536−3544.
(42) Mena-Morcillo, E.; van der Zalm, J.; Chen, A. Spatially Resolved Optical Spectroscopic Measurements with Simultaneous Photoelectrochemical Mapping Using Scanning Electrochemical Probe Microscopy. *J. Phys. Chem. Lett.* **2023**, *14* (19), 4600−4606.
(43) Takahashi, Y.; Kumatani, A.; Shiku, H.; Matsue, T. Scanning Probe Microscopy for Nanoscale Electrochemical Imaging. *Anal. Chem.* **2017**, *89* (1), 342−357.
(44) de Oliveira, G. A.; Kim, M.; Santos, C. S.; Limani, N.; Chung, T. D.; Tetteh, E. B.; Schuhmann, W. Controlling Surface Wetting in High-Alkaline Electrolytes for Single Facet Pt Oxygen Evolution Electrocatalytic Activity Mapping by Scanning Electrochemical Cell Microscopy. *Chem. Sci.* **2024**.
(45) *Standard Practice for Preparing, Cleaning, and Evaluating Corrosion Test Specimens*. https://www.astm.org/g0001-03r17e01.html (accessed 2024−07−09).
(46) Tetteh, E. B.; Krysiak, O. A.; Savan, A.; Kim, M.; Zerdoumi, R.; Chung, T. D.; Ludwig, A.; Schuhmann, W. Long-Range SECCM Enables High-Throughput Electrochemical Screening of High Entropy Alloy Electrocatalysts at Up-To-Industrial Current Densities. *Small Methods* **2024**, *8* (7), 2301284.
(47) Aricò, A. S.; Bruce, P.; Scrosati, B.; Tarascon, J.-M.; van Schalkwijk, W. Nanostructured Materials for Advanced Energy Conversion and Storage Devices. *Nat. Mater.* **2005**, *4* (5), 366−377.

https://doi.org/10.1021/acsmeasuresciau.4c00042
ACS Meas. Sci. Au 2025, 5, 178−188